Description of ALF3D code.

The code solves fully three-dimensional time-dependent compressible MHD equations under the assumption of dipole magnetic filed in the co-rotating frame of reference. The magnetic dipole is assumed to be aligned with the rotation axis. For each of the three evolutionary scenarios, we assume that the solar wind is driven by a combination of the thermal pressure gradient and Alfvén waves generated at the coronal wind base. The initial and boundary conditions for the current Sun simulations are similar to those described in Usmanov et al. (2014). The computational domain in our wind model is sub-divided into three separate regions. The first, inner wind region, extends from 1 to 20 $R\odot$ ($R\odot$ is the solar radius). In this region, the solar corona is described in the single-fluid polytropic approximation, with the polytropic index $\gamma = 1.08$ or as nearly isothermal plasma. The outer boundary of the inner region is set at 20 $R\odot$ to assure that the solar wind flow at the boundary is supersonic and super-Alfvénic. We obtain a steady-state solution for the transonic and trans-Alfvénic single-fluid coronal wind by using the time-relaxation method described by Usmanov et al. (2000). The inner boundary conditions specified at the wind base, $r = 1$ $R\odot$, are updated in the course of the relaxation process to be consistent with the flow characteristics near the coronal boundary (Usmanov et al. 2000). They evolve to a steady state simultaneously with the solution in the inner region. The outflow boundary conditions at 20 $R\odot$ are approximated by a first-order (linear) extrapolation. In the second region extending between 20 $R\odot$ and 0.3 AU, the solar wind flow is supersonic and super-Alfvénic. In this region, the adiabatic index $\gamma = 5/3$ is used in combination with Hollweg's electron heat flux (Hollweg 1974, 1976). Because plasma in the second region (at heights >20 $R\odot$) is collisionless, we apply a two-fluid approximation including thermal electrons and protons to describe the solar wind. A steady-state solution in this region is constructed using a marching-along-radius numerical method (Pizzo 1978, 1982; Usmanov 1993).
The third, outer wind region starts at 0.3 AU and covers the heliosphere up to 100 AU, where plasma is treated as three-fluid plasma composed of electrons, thermal protons and pickup protons. This is critical in correctly calculating the wind velocity due to interaction with the incoming interstellar hydrogen. In this region, in order to describe the Alfvén wave driven solar wind turbulence and associated plasma heating rate, we decompose plasma quantities including plasma pressure, velocity and magnetic field into the Reynolds averaged and fluctuating components (see Usmanov et al. 2014) and use the turbulence transport equations with an eddy-viscosity approximation for the Reynolds stress tensor and turbulent electric field. We then obtain steady-state solutions using time relaxation that incorporates boundary conditions from the intermediate (the second) region.

APPLICATION OF ALF3D FOR WINDS FROM THE YOUNG SUN.

ALF3D was applied our solar wind model in the region from the coronal wind base to 3 AU for three wind evolutionary scenarios, M1, M2, and M3, reproducing the conditions in the early Sun at 0.7 Gyr with the rotation period of 5 days (at equator), the

intermediate-age Sun at 2 Gyr with the rotation period of 10 days, and the wind model for the current Sun with the rotation period of 25 days (Airapetian & Usmanov 2016).

Figure 1 presents the latitudinal distribution of the wind radial velocity for the M1 (red), M2 (blue), and M3 (green) scenarios. The bi-modal wind distribution in the three evolutionary scenarios represents the result of the self-consistent solution from out model that assumes a simple dipole magnetic field.

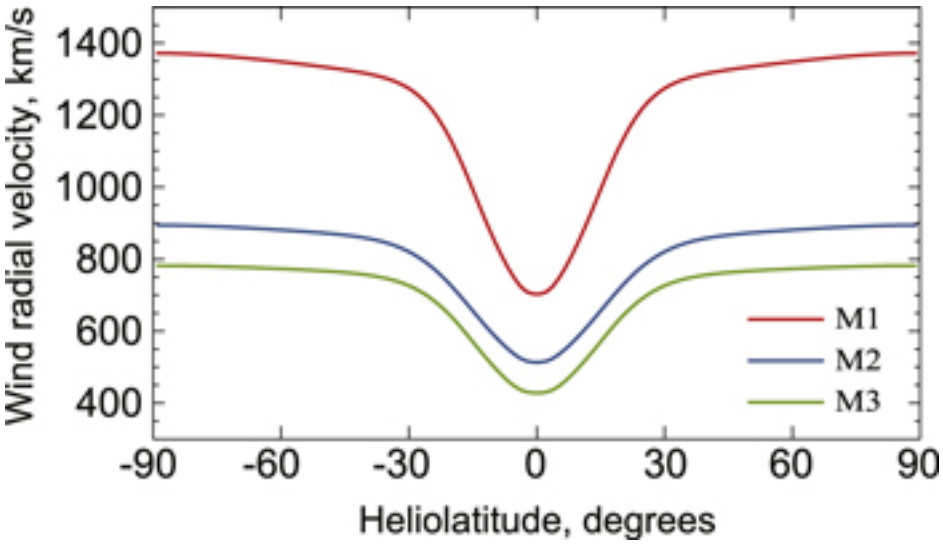

Zoom In Zoom Out Reset image size

Figure 1. Latitudinal distribution of the solar wind radial velocity at 1 AU. The red, blue and green curves represent the wind's velocity profiles from the young Sun at 0.7 Gyr (M1 scenario), the intermediate age Sun at 2 Gyr (M2 scenario), and the current Sun (M3 scenario), respectively.

Figure 2 shows the radial profiles of the high latitude fast wind's radial velocity between the wind base and 20 $R\odot$ for the M1 (red), M2 (blue), and M3 (green) scenarios. The figure shows that the resulting steady-state solution for the terminal wind velocity for the young Sun is a factor of 2 greater than for the current Sun.

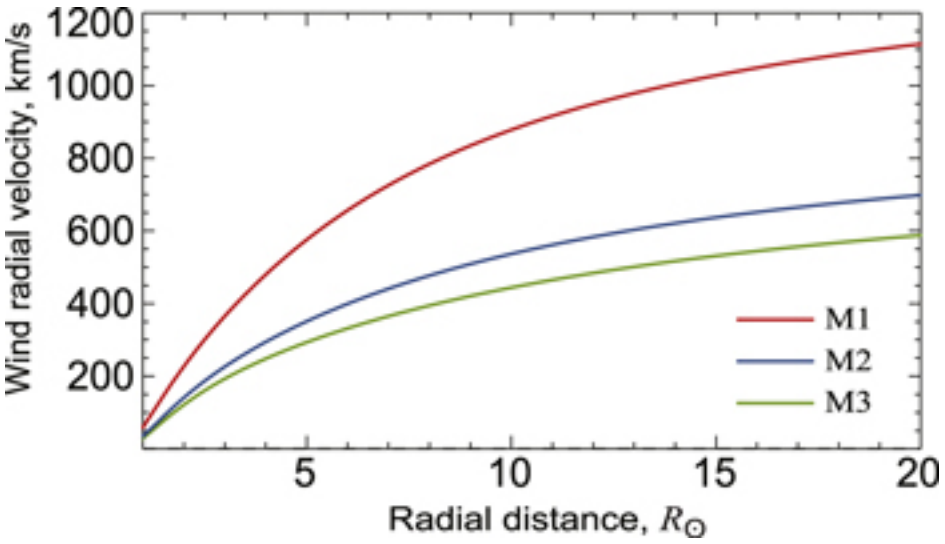

Zoom In Zoom Out Reset image size

Figure 2. Radial profiles of the high altitude fast solar wind radial velocity. The red, blue and yellow curves describe the wind's velocity profile from the wind base to 20 $R\odot$ for the models of the young Sun at 0.7 Gyr (M1 scenario), the intermediate age Sun at 2 Gyr (M2 scenario), and the current Sun (M3 scenario), respectively.

Figure 3 shows the proton temperature in the fast wind for the M1, M2, and M3 scenarios from 0.3 to 1 AU. The figure shows that the proton temperature of the paleo solar wind is 5.5×10^5K, which is twice as hot as that of the current solar wind.

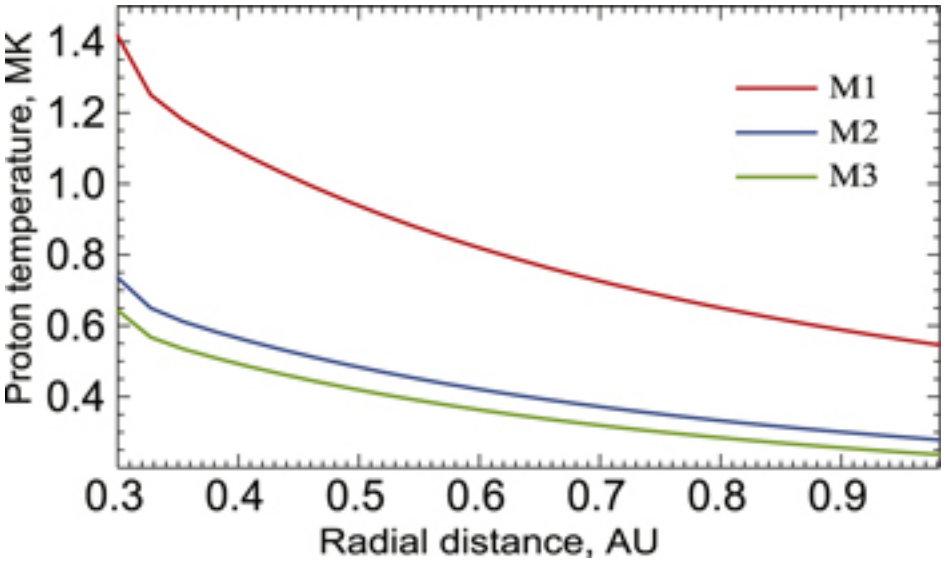

Figure 3. Radial profiles of the proton temperature in the fast wind. The red, blue, and green curves describe the wind's temperature profiles for the models of the young Sun at 0.7 Gyr (M1 scenario), the intermediate age Sun at 2 Gyr (M2 scenario), and the current Sun (M3 scenario), respectively.

Figure 4 presents the total mass-loss rates from the fast and slow wind components calculated for the M1, M2, and M3 scenarios superimposed on the range of empirically

derived mass-loss rates for solar-like stars at various phases of evolution (Wood et al. 2005).

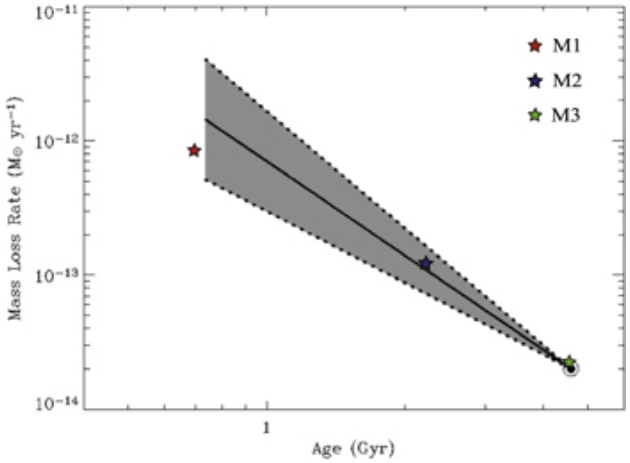

Figure 4. Total mass-loss rates from Alfvén-wave driven solar winds at 0.7 Gyr (red star), 2 Gyr (blue star), and 4.6 Gyr (green star) superimposed on the empirically derived values of mass-loss rates (gray area) from a sample of solar-type stars of various ages (Wood et al. 2005).